A&A 498, 811–820 (2009)
DOI: 10.1051/0004-6361/200810812

Astronomy & Astrophysics

Spectral and temporal variations of the isolated neutron star RX J0720.4−3125: new XMM-Newton observations⋆

M. M. Hohle[1,2], F. Haberl[1], J. Vink[3], R. Turolla[4,5], V. Hambaryan[2], S. Zane[5], C. P. de Vries[6], and M. Méndez[7,8]

[1] Max-Planck-Institut für extraterrestrische Physik, Giessenbachstrasse, 85741 Garching, Germany
[2] Astrophysikalisches Institut und Universitäts-Sternwarte Jena, Schillergässchen 2-3, 07745 Jena, Germany
e-mail: mhohle@astro.uni-jena.de
[3] University Utrecht, PO Box 80000, 3508 TA Utrecht, The Netherlands
[4] Department of Physics, University of Padua, via Marzolo 8, 35131 Padova, Italy
[5] Mullard Space Science Laboratory, University College London, Holmbury St. Mary, Dorking, Surrey, RH5 6NT, UK
[6] SRON, Netherlands Institute of Space Research, Sorbonnelaan 2, 3584 CA, Utrecht, The Netherlands
[7] Kapteyn Astronomical Institute, University of Groningen, PO Box 800, 9700 AV Groningen, The Netherlands
[8] Astronomical Institute Anton Pannekoek, University of Amsterdam, Kruislaan 403, 1098 SJ Amsterdam, The Netherlands

Received 15 August 2008 / Accepted 14 February 2009

ABSTRACT

Context. In the past, the isolated, radio-quiet neutron star RX J0720.4−3125 showed variations in its spectral parameters (apparent radius, temperature of the emitting area and equivalent width of the absorption feature) seen in the X-ray spectra, not only during the spin period of 8.39 s, but also over time scales of years. New X-ray observations of RX J0720.4−3125 with XMM-Newton extend the coverage to about 7.5 years with the latest pointing performed in November 2007. Out of a total of fourteen available EPIC-pn datasets, eleven have been obtained with an identical instrumental setup (full frame read-out mode with a thin filter), and are best suited for a comparative investigation of the spectral and timing properties of this enigmatic X-ray pulsar.
Aims. We analysed the new XMM-Newton observations together with archival data in order to follow the spectral and temporal evolution of RX J0720.4−3125.
Methods. All XMM-Newton data were reduced with the standard XMM-SAS software package. A systematic and consistent data reduction of all these observations is warranted in order to reduce systematic errors as far as possible.
Results. We investigate the phase residuals derived from data from different energy bands using different timing solutions for the spin period evolution and confirm the phase lag between hard and soft photons. The phase shift in the X-ray pulses between hard and soft photons varies with time and changes sign around MJD = 52 800 days, regardless of the chosen timing solution. The phase residuals show a marked dependence on the energy band, and possibly follow a cyclic pattern with a period of ∼9–12 yrs. We find that an abs(sine) dependence provides a better fit to the residuals with respect to a simple sine wave, although in both cases the reduced χ^2 is not completely satisfactory. We compared the model fit to phase residuals derived from EPIC-MOS and Chandra (HRC and ACIS) data restricted to the hard energy band (400–1000 eV) to take into account the different energy responses of these instruments.
Conclusions. The new data are not in contradiction with RX J0720.4−3125 being a precessing neutron star but do not provide overwhelming evidence for this picture either.

Key words. stars: individual: RX J0720.4−3125 – stars: neutron – stars: magnetic fields – X-rays: stars

1. Introduction

The radio quiet, isolated neutron star RX J0720.4−3125 was discovered in ROSAT all-sky survey data (Haberl et al. 1997). It belongs to a group of seven neutron stars with similar properties often called the magnificent seven, hereafter M7. The X-ray spectra are well represented by a blackbody model (with absorption features in some cases) without any additional non-thermal component. For the two brightest stars (RX J1856.5-3754 and RX J0720.4−3125) the trigonometric parallax was measured (Kaplan et al. 2007) which enables us to estimate the size of the emission region. Six of them are X-ray pulsars with relatively long periods between 3.5 s and 11.4 s (for a review see, e.g., Haberl 2007). From the spin period, period derivative ($\dot{P}$) and the energy of absorption lines one can independently estimate the magnetic field strength on the surface of the neutron star. Both methods consistently suggest strong magnetic fields in excess of $\sim 10^{13}$ Gauss (Haberl 2005). The properties of the M7 make them of special interest for the investigation of cooling models of neutron stars (see Page & Reddy 2006; Page et al. 2006; and Blaschke & Grigorian 2007) and for constraining of the equation of state of matter at nuclear densities (Trümper et al. 2004).

RX J0720.4−3125 shows a long term variation in its spectral parameters (see de Vries et al. 2004; Vink et al. 2004; and Haberl et al. 2006, hereafter H06), i.e. its temperature, size of the emitting area and equivalent width of the absorption feature. The variations derived from data covering 5.5 years were consistent with a period of about (7.1 ± 0.5) yr, when assuming a sinusoidal shape of the variations (H06). Kaplan & van Kerkwijk (2005, hereafter KvK05) performed a coherent timing analysis

⋆ Based on observations with XMM-Newton, an ESA Science Mission with instruments and contributions directly funded by ESA Member states and the USA (NASA).

Table 1. XMM-Newton EPIC observations of RX J0720.4−3125.

Orbit	Observation	Date	MJD	EPIC instrument setup[1]			Duration [s]
			[days]	pn	MOS1	MOS2	(EPIC-pn)
78	0124100101	2000 May 13	51 677	FF thin	FF thin	SW thin	62 498
175	0132520301	2000 Nov. 21–22	51 869	FF medium	SW thin	–	26 118
533	0156960201	2002 Nov. 6–7	52 584	FF thin	FF thin	FF thin	28 373
534	0156960401	2002 Nov. 8–9	52 586	FF thin	FF thin	FF thin	30 173
622	0158360201	2003 May 2–3	52 761	SW thick	FF thin	FF thin	72 796
711	0161960201	2003 Oct. 27	52 939	SW medium	FF thin	FF thin	43 013
815	0164560501	2004 May 22–23	53 147	FF thin	FF thin	FF thin	43 951
986	0300520201	2005 April 28	53 488	FF thin	SW thin	SW thin	51 435
1060	0300520301	2005 Sep. 23	53 635	FF thin	SW thin	SW thin	51 135
1086	0311590101	2005 Nov. 12–13	53 686	FF thin	SW thin	SW thin	37 835
1181	0400140301	2006 May 22	53 877	FF thin	SW thin	SW thin	20 035
1265	0400140401	2006 Nov. 05	54 044	FF thin	SW thin	SW thin	20 035
1356	0502710201	2007 May 05	54 225	FF thin	FF thin	FF thin	20 035
1454	0502710301	2007 Nov. 17	54 421	FF thin	FF thin	FF thin	23 059

[(1)] Read – out mode and filter; FF; Full Frame; SW; Small Window.

for RX J0720.4−3125 by including all data (ROSAT, XMM-Newton and Chandra) available at that time. This enabled them to determine the period more accurately then previous studies (Cropper et al. 2001; Zane et al. 2002; and Kaplan et al. 2002). In their Table 2 KvK05 provide two different values for a constant $\dot{P}$: 7.016×10^{-14} s/s for Chandra data only and 6.983×10^{-14} s/s using all data. By applying these timing solutions to derive phase binned light curves, KvK05 obtained phase residuals. These phase residuals, as shown by H06, can be modeled by a sinusoidal function with a period of (7.7 ± 0.6) yr. This is consistent with the (7.1 ± 0.5) yr period of the spectral variations. As a possible explanation for the behaviour of RX J0720.4−3125, de Vries et al. (2004) and H06 suggested precession of the neutron star. van Kerkwijk et al. (2007, hereafter vK07) derived a new $\dot{P} = 6.957 \times 10^{-14}$ s/s including new XMM-Newton and Chandra data, but still obtained sinusoidal-like phase residuals. KvK05 and vK07 derived $\chi^2 = 1$ for their timing solutions only after adding an artificial uncertainty to the time of arrivals (see KvK05 and vK07 for more details). Furthermore, they add a glitch model to the spin-down term and claim the occurrence of the glitch around MJD = 52 800 days to explain the timing and spectral changes of this neutron star. Equivalent to the glitch model vK07 found a period ≈4.3 yr but that is not consistent with the period ≈7.5 yr found by H06. On the other hand, the data set used in H06 (EPIC-pn) is quite different to that used in vK07 (also including EPIC-MOS1 & MOS2 and Chandra HRC-S/LETG).

This paper includes new data from the recent XMM-Newton (Jansen et al. 2001) observations which are part of an ongoing monitoring programme, and Chandra archival data. We discuss our results as new evidence for a cyclic behaviour of RX J0720.4−3125 based on timing solutions from KvK05 and vK07.

2. X-ray observations and timing analysis

Since the work of Haberl (2007) was published, four new XMM-Newton observations have been performed between May 2006 and November 2007 at six month intervals (satellite revolutions 1181, 1265, 1356 and 1454). All new EPIC-pn (Strüder et al. 2001) observations were executed with the same instrument setup in full frame mode and with thin filter (see Table 1 for a summery of the observations). Inclusion of the latest pointings brings the number of available EPIC-pn datasets to fourteen. These, in conjunction with the MOS (Turner et al. 2001) data (see Table 1 for details on the instrumental setup), have been used for the source timing analysis. All observations were reduced with the XMM-Newton Science Analysis System (SAS) version 7.1.0.

To derive the phase residuals from a certain timing solution, we binned the light curve in 40, 100 and 400 phase bins. The number of phase bins did not influence the result. Considering the time resolution of the full frame (2.6 s) and small window mode (0.3 s) we divide the MOS light curves in 10 and 40 phase bins, respectively. Phase residuals from all observations are obtained fitting a sinusoidal function to the pulse profile. The uncertainties of the phase residuals are derived from the uncertainties of the sinusoidal fit. All errors on the phase residuals in this paper correspond to 1σ.

In the analysis of KvK05 the phase residuals for the last observations show an increasing trend while in the case of vK07 (with more data included) the trend is reversed. Therefore, the timing solution for RX J0720.4−3125 strongly depends on the behaviour of the source in the future and all solutions obtained so far must be regarded as preliminary. Hence, in the following we examine phase residuals for two timing solutions provided by KvK05 and vK07 (in both cases their "all data" solution).

To reduce systematic effects due to the changing low-energy response of the EPIC-MOS cameras we use only events from the 400–1000 eV band for MOS (the 120–1000 eV band is used for pn). The phase residuals using the coherent timing solution of KvK05 are shown in Fig. 1. As already mentioned in Haberl (2007), systematic differences between phase residuals from different instruments can be seen, which are probably caused by the energy dependent pulse profile. To verify this, we investigated the phase residuals for two different bands (soft: 120–400 eV and hard: 400–1000 eV) using EPIC-pn data, and the results are shown in Fig. 2. The phase residuals exhibit a clear energy dependence while the phase shift between the two bands varies with time and changes sign around MJD = 52 800 days. As an example of a relatively large phase shift between hard and soft bands we show the pulse profile for satellite orbit 986 in Fig. 3. The phase shift is clearly visible and the trend is much the same as in Fig. 2 if we add or subtract the error of $\dot{P}$ provided in KvK05.

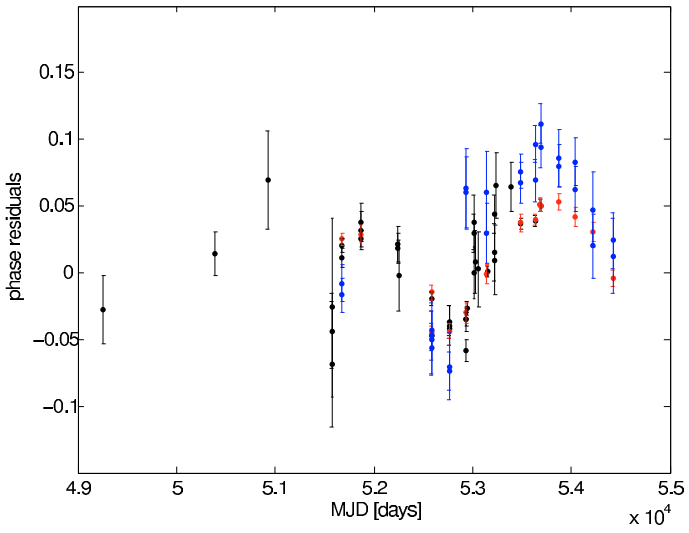

Fig. 1. Phase residuals of RX J0720.4−3125 derived from the timing solution from Kaplan & van Kerkwijk (2005). Red dots: refer to EPIC-pn data, blue dots: to EPIC-MOS1 & MOS2 observations, black dots: reproduced from the original solution of Kaplan & van Kerkwijk (2005).

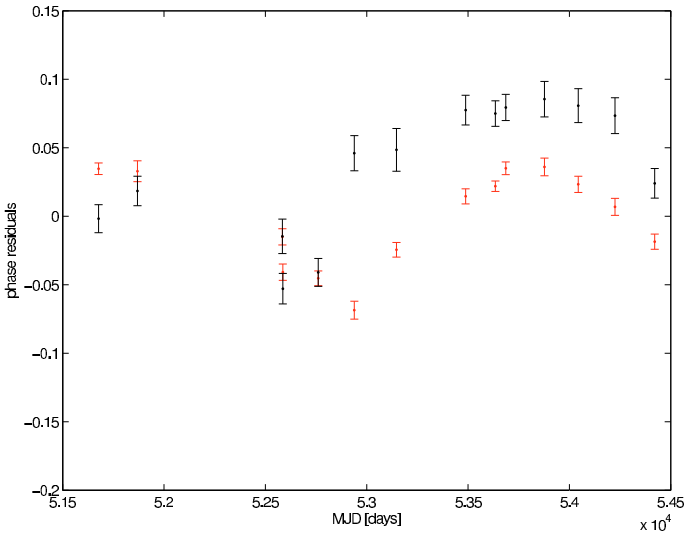

Fig. 2. Phase residuals of RX J0720.4−3125 derived from EPIC-pn data with the timing solution from Kaplan & van Kerkwijk (2005) in the soft band (120–400 eV, red) and hard band (400–1000 eV, black).

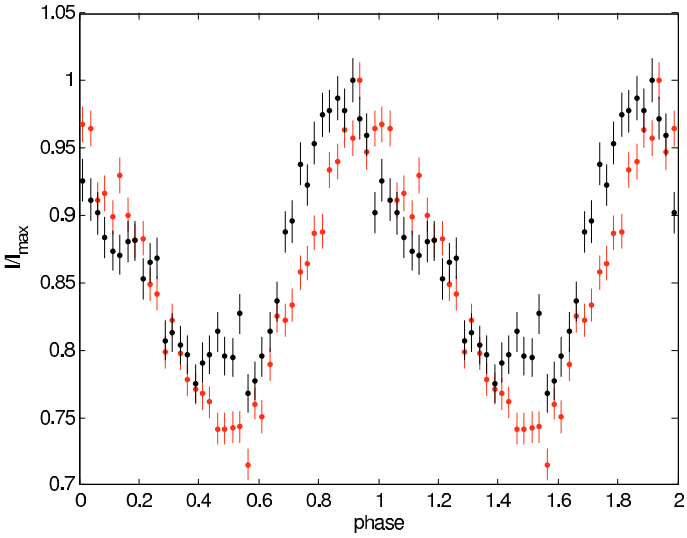

Fig. 3. Phase shift of hard (black) and soft (red) band of RX J0720.4−3125 derived from EPIC-pn data (satellite orbit 986) with the timing solution from Kaplan & van Kerkwijk (2005). Errors are Poissonian. The y-axis denotes the relative counts per phase bin.

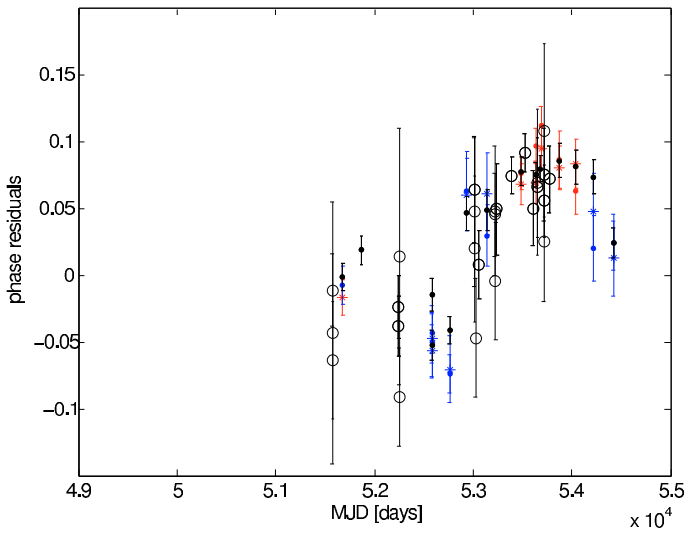

Fig. 4. Phase residuals of RX J0720.4−3125 derived from the timing solution from Kaplan & van Kerkwijk (2005). Black dots: EPIC-pn, red dots: EPIC-MOS1 small window and thin filter, red stars: EPIC-MOS2 small window and thin filter, blue dots: EPIC-MOS1 full frame and thin filter, blue stars: EPIC-MOS2 full frame and thin filter (all in hard band); open circles show phase residuals from Chandra HRC (no energy selection) and ACIS (hard band).

We also applied the timing solution from KvK05 to archival Chandra HRC-S/LETG (zeroth order) and ACIS data (for details of the observations see KvK05 and vK07). For observations 368, 369, 745, 2771, 2772, 4667, 4668, 4669, 4670, 4671, 4672, 7177, 7243 and 7245 we use 10 phase bins and 40 phase bins for the other observations because of the different time resolution and number of photons. Considering the energy dependence of the phase residuals we restrict the energy band for the analysis of the ACIS data to the hard band (400–1000 eV). We show all phase residuals from Chandra and XMM-Newton observations in Fig. 4. Comparison with Fig. 1 shows that the agreement between the different instruments is much improved.

As in the EPIC-pn observations before (see Haberl 2007; H06; and de Vries et al. 2004), the pulse profile can be approximated by a sinusoid. In Fig. 5 we show the pulse profiles for the last four EPIC−pn data sets together with the hardness ratios. The hardness ratios $HR = H/S$ are anti-correlated with intensity. The pulse phases were derived by applying the "all data" solution of KvK05 (2005). The light curves look the same, except for absolute phase of course, using the timing solution of vK07. As noted before, the profiles are not exactly sinusoidal and look somewhat skewed. This is particularly true for the latest observations. To explore how much the behaviour of the residuals is influenced by the choice of the pulse shape we also tried a sawtooth profile, in which the location and the height of the minimum are free to vary. Results for the phase residuals in the two bands (see Fig. 6) are similar to those derived for a sinusoidal profile. This supports the fact that energy-dependent phase residuals are indeed present and do not depend on the chosen shape of the pulse profile. We note that the χ^2/d.o.f. values of the sine fits shown in Fig. 5 are smaller than those of the sawtooth fits (χ^2/d.o.f. = 2.94, 4.06, 3.70, 2.50 in the order of increasing

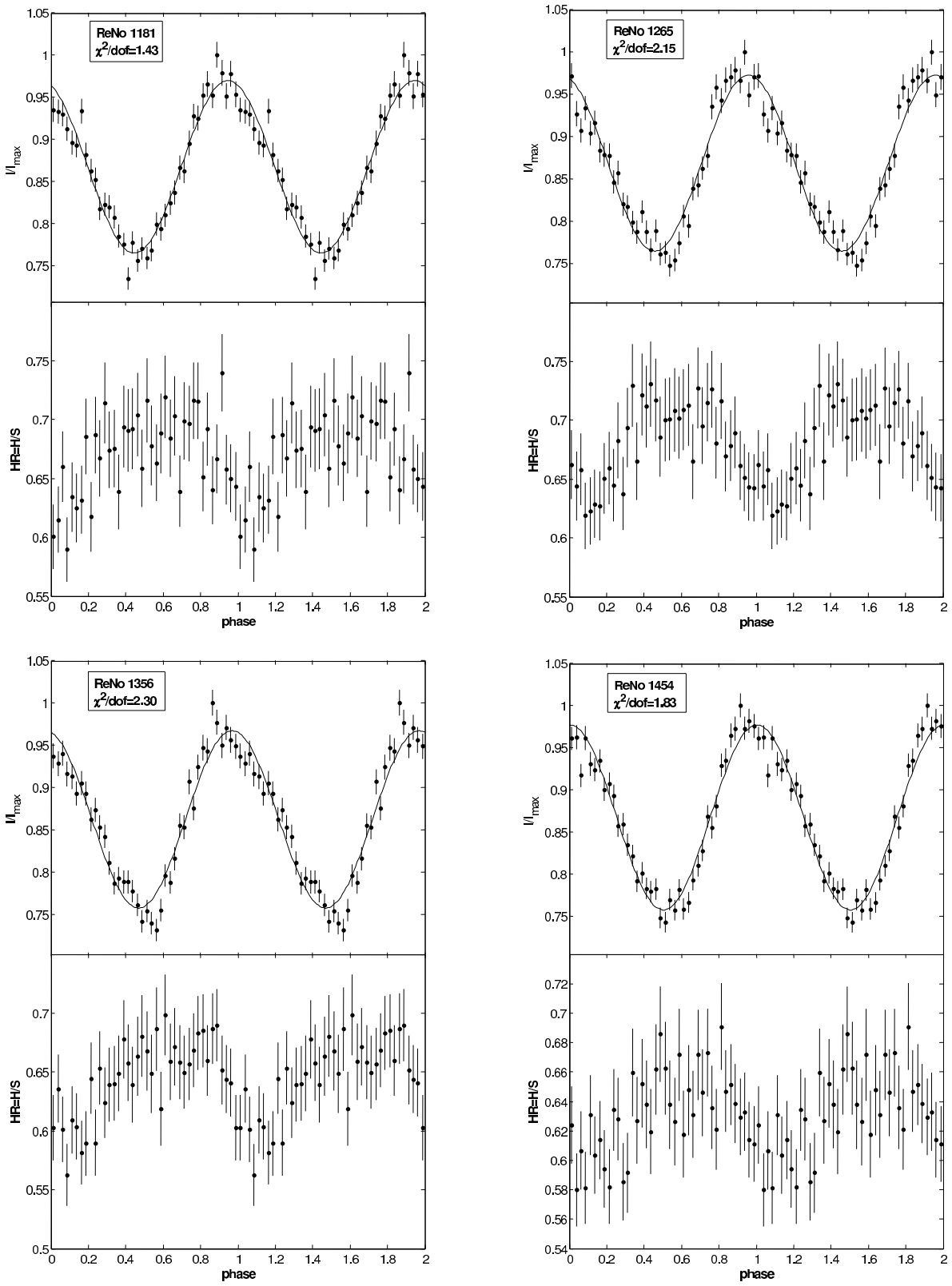

Fig. 5. Folded EPIC-pn pulse profile (120−1000 eV, 40 phase bins, d.o.f. = 37 in all cases) with sinusoidal fit and hardness ratio $HR = H/S$ (bands described in the text) of the last four observations. Pulse phases are obtained by applying the "all data" solution of Kaplan & van Kerkwijk (2005). Errors are Poissonian. $I/I_{\max}$ denotes the relative counts per phase bin.

revolution number) so that a sine wave provides a better interpretation of the data, although the quality of the fits is still not satisfactory. For all fits d.o.f. = 37.

The timing solution of vK07 with a glitch at MJD = 52 817 days produces phase residuals three times larger than those seen in Fig. 2 with a large scatter and will not be

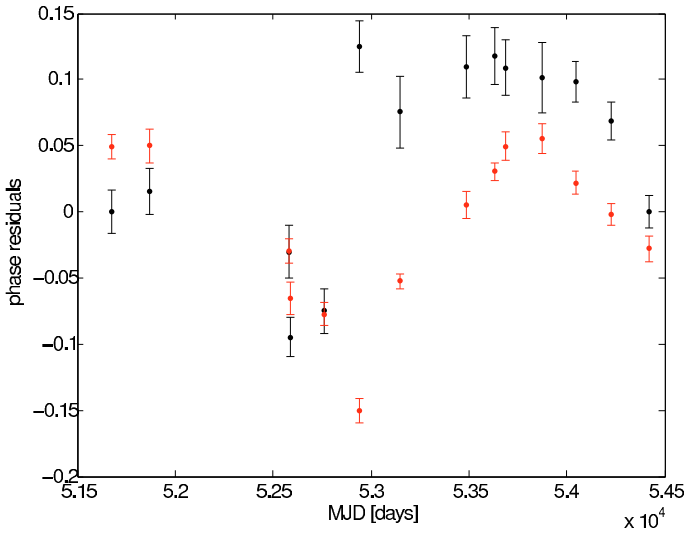

Fig. 6. Phase residuals of RX J0720.4−3125 derived from the timing solution from Kaplan & van Kerkwijk (2005), similar to those in Fig. 2, but fitting a sawtooth instead of a sinusoidal to the pulse profile.

considered any further. The pulse profiles for EPIC−pn satellite orbit 622 and 711 in both energy bands in Fig. 7 are an example of the large phase shifts from one observation to the next by applying this solution.

3. Modeling the long term evolution of the timing properties

From the first XMM-Newton observations of RX J0720.4−3125 Cropper et al. (2001) reported a phase shift between X-ray intensity and hardness ratio (HR, hard and soft band count ratio). Furthermore, de Vries et al. (2004) found that the phase shift changed sign between the year 2000 (the HR leads the intensity profile) and 2003 (the HR lags behind the intensity). As can be seen in Fig. 2 this occurred around MJD = 52 800 days. Since then, the hard band emission lags behind the soft band emission and the shift seems to decrease again from a maximum of ∼0.1. The phase lag dependence on the energy bands clearly shows that using data from instruments with different energy-dependent sensitivity may introduce systematic errors in the timing analysis. The EPIC-pn instrument has a high low-energy response relative to the hard band, therefore Chandra ACIS and EPIC-MOS are expected to be closer to the EPIC-pn results restricted to the hard band.

As in previous work, we start modeling the phase residuals using a sine wave function (Fig. 8, top). To avoid systematic effects we use only the EPIC-pn data (120–1000 eV) for our timing analysis. The different period derivatives, $\dot{P}$, given in KvK05 and vK07 depend on which and how many data points and from which instruments they were used. We already mentioned the different energy response of the different instruments. $\dot{P}$ depends on how much of the cycle, shown in Fig. 1, is covered with observations and can be determined more accurately only in the future, when at least one full cycle of the variation of the phase residuals is observed, assuming a 10–12 yr period as discussed below. Therefore, we introduced an additional linear term $y = mt + n$, as can be seen in Fig. 8 for the timing solution of KvK05 (middle) and that of vK07 with constant spin-down without glitches (bottom).

The two maxima in the phase residuals (Fig. 8) do not necessarily have equal heights. By adding the linear term, we

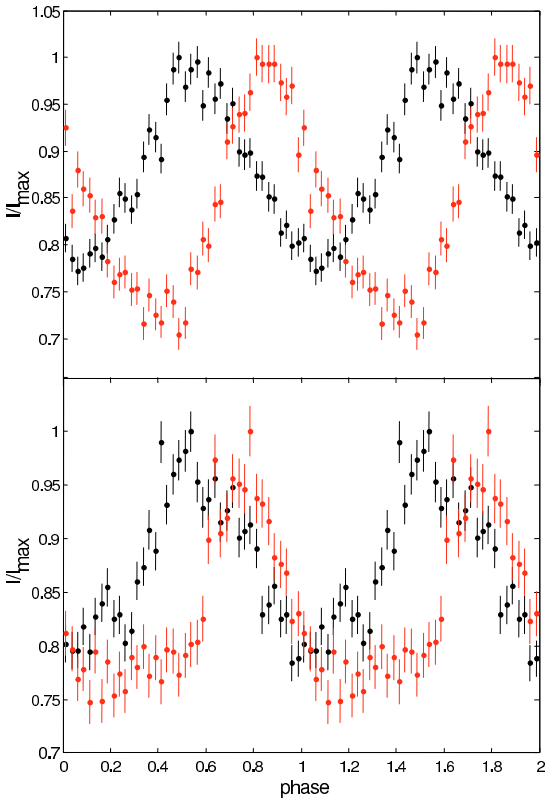

Fig. 7. Pulse profiles of satellite orbit 622 (black) and 711 (red) in soft (*upper panel*) and hard (*lower panel*) bands as an example for the large phase shift applying the timing solution from vK07 with a glitch. The phase residuals are much larger than for the other timing solutions (discussed in the text) and the pulse profile looks more skewed. Error bars denote Poissonian errors. On the vertical axis are the counts are normalized to their maximum value.

automatically take into account the different values of $\dot{P}$ and a possible different amplitude of the two maxima covered by the observations. For the three cases described above, we derive periods of (5.58 ± 0.33) yr, (7.20 ± 1.50) yr and (5.59 ± 0.57) yr, respectively (here and below, errors on the periods correspond to 1σ). The values are consistent within their errors and in particular the first and last value are nearly identical. This is expected because a possible period should not significantly depend on the actual timing solution (as long as this is correct to first order). It should be noted, however, that the fits with a sine wave are formally not acceptable, given the derived χ^2 values. The unacceptable fit can be partly explained by the two data points from MJD = 52 584 and 52 586 days. It suggests that the sine wave is not a good representation of the data. We excluded the data point from MJD = 52 584 days and derived periods of (6.54 ± 0.14), (6.55±0.46) and (5.73±0.43) yr, respectively, for the three cases, while the values for χ^2/d.o.f. are 17.16/9, 16.90/8 and 35.12/8, respectively. Only the fit with the data shown in Fig. 8 (top), excluding the data point at MJD = 52 584 days, is formally acceptable. The reason for the outlier at this epoch is unclear.

In the first observation the soft photons lag behind the hard photons, while in the observations after MJD = 52 800 days the opposite is true (see Fig. 2). The phase lag in the first observation is supported by Fig. 2 of de Vries et al. (2004), which is independent of a model fit to the pulse profile. The energy dependent heights of the two phase residual maxima (Fig. 2) show that the actual period of the modulation could be twice the sine period. The energy dependence suggests a model of emission

Table 2. Periods derived from the fits of the phase residuals with a model consisting of abs(sine)+mt+n for different timing solutions.

Model	Timing solution	period [yr]	m [phase res./s]	amplitude [phase res.]	offset (n) [phase res.]	χ^2	d.o.f.	χ^2/d.o.f.
			revolution 622 excluded					
A1	KvK05	15.21 ± 0.65	0	0.163 ± 0.068	–0.079 ± 0.017	24.51	9	2.72
A2	KvK05	15.210 ± 0.011	7.45×10^{-11}	0.15 ± 0.36	–0.41 ± 3.40	22.75	8	2.84
A3	vK07	12.488 ± 0.055	-1.10×10^{-11}	0.125 ± 0.034	–0.01 ± 0.41	64.49	8	8.06
A4	vK07	10.693 ± 0.059	0	0.065 ± 0.028	–0.015 ± 0.015	61.53	9	6.84
			doubled error of revolution 622					
B1	KvK05	10.711 ± 0.058	0	0.097 ± 0.050	–0.028 ± 0.035	122.45	10	12.25
B2	KvK05	11.504 ± 0.072	39.21×10^{-11}	0.099 ± 0.029	–1.83 ± 0.40	21.87	9	2.43
B3	vK07	10.546 ± 0.069	3.44×10^{-11}	0.095 ± 0.034	–0.20 ± 0.42	44.89	9	4.99
B4	vK07	9.656 ± 0.023	0	0.057 ± 0.026	–0.012 ± 0.017	51.38	10	5.14
			doubled error of revolution 175, 622 and 711					
C1	KvK05	9.07 ± 0.14	0	0.058 ± 0.068	0.003 ± 0.042	138.33	10	13.83
C2	KvK05	9.376 ± 0.037	45.17×10^{-11}	0.087 ± 0.035	–2.09 ± 0.48	18.45	9	2.05
C3	vK07	9.009 ± 0.037	2.48×10^{-11}	0.090 ± 0.040	–0.15 ± 0.53	32.61	9	3.62
C4	vK07	9.017 ± 0.038	0	0.076 ± 0.031	–0.025 ± 0.019	45.00	10	4.50

The plots for models B1-3 are shown in Fig. 9. All errors correspond to 1σ.

originating from two hot spots with different temperature. In the case of a precession model, for one half of the precession period the soft emission (cooler pole) would precede the hard emission and for the other half it would be the other way around. The cooler cap would be mostly visible for half the precession cycle, while in the other half the hotter cap would dominate emission. If the emission arises in different poles this suggests that the profile should be that of an abs(sine), similar to that used by vK07 and van Kerkwijk & Kaplan (2007) but with a different interpretation. They found a period ≈4.3 yr as a solution equivalent to the glitch model. Unfortunately van Kerkwijk & Kaplan (2007) do not provide errors, and we cannot check if our value of the period ≈5.5 yr is consistent with theirs. The difference of the values may be explained by the four new EPIC-pn observations we add.

We interpret the turn-around in the phase residual evolution (near MJD = 52 800 days) not as a glitch, but as "switching" of the emission to the predominantly visible pole. As in the fit with the normal sine function, we again add the linear term to the abs(sine). To reduce systematic effects due to the use of different filters we use the EPIC-pn hard band (400–1000 eV) data. We use the hard band in order to be able to include data from other instruments, although statistics in the soft band would be preferable. For the fit we further increase the size of the error of the phase residual in revolution 622 by a factor of two (model B1–B4). This observation was performed with the thick filter, which has a significantly lower transmission in the soft energy band compared to the medium and thin filter. This causes a systematic shift of this phase residual to larger values and would introduce systematic errors in the fit results. Excluding this observation completely (model A1–A4), we obtained a period which is 2–4.5 years longer (see Table 2). To get an estimate of the systematic error of the period, which is likely larger than the statistical error derived from the fit, we also applied a doubled error for all observations which were not performed with the thin filter, i.e. revolutions 175, 622 and 711 (model C1–C3). The results of the fitting procedures are listed in Table 2 and plotted in Fig. 9. Except for model A, the advantage of introducing an additional slope is clearly visible in the χ^2/d.o.f. as compared to the poor fits without a slope.

Applying a sine instead of the abs(sine) models B1, B2 and B3, we derive χ^2/d.o.f. = 3.31, 3.67 and 4.85, compared to 12.25 (top), 2.43 (middle) and 4.99 (bottom) in Fig. 9. The fit of model B1 is much better with a sine instead of an abs(sine) but a better approximation would be an abs(sine) with an additional slope, which gives the best χ^2 = 2.43 (B2) in this case for the timing solution of KvK05. The two χ^2 values for the timing solution of vK07 are not significantly different.

For a consistency check we show in Fig. 10 the abs(sine) model fit shown in Fig. 9 (middle) together with the phase residuals obtained from EPIC-pn, EPIC-MOS and ACIS (all hard band) and HRC observations. We excluded in this figure Chandra data points with errors ≥0.03.

Table 3. All EPIC-pn observations in full frame mode with the thin filter of RX J0720.4−3125 with the derived variations of the pulse averaged spectra.

Orbit	MJD	kT [eV]	EW [eV]	radius [km]
78	51 677	86.5 ± 0.4	–4.0 ± 4.0	4.79 ± 0.09
175	*51 870*	*86.0 ± 0.7*	*+5.6 ± 7.0*	*4.90 ± 0.14*
533/534	52 585/7	88.4 ± 0.4	–16.8 ± 3.3	4.70 ± 0.07
711	*52 940*	*92.0 ± 0.6*	*–64.7 ± 5.4*	–
815	53 148	94.6 ± 0.5	–58.6 ± 4.2	4.29 ± 0.08
986	53 489	94.3 ± 0.4	–57.8 ± 3.8	4.35 ± 0.07
1060	53 636	93.7 ± 0.5	–55.0 ± 3.8	4.37 ± 0.08
1086	53 687	93.1 ± 0.5	–55.9 ± 3.8	4.50 ± 0.08
1181	53 877	93.1 ± 0.6	–51.2 ± 4.8	4.44 ± 0.10
1265	54 045	92.7 ± 0.6	–53.6 ± 4.7	4.53 ± 0.11
1356	54 226	92.4 ± 0.6	–44.1 ± 4.9	4.45 ± 0.11
1454	54 421	91.8 ± 0.6	–44.6 ± 4.6	4.50 ± 0.10

Observations done in different observing modes, which were not used for the fit are in italic. The radius obtained from observation 711 is not used at all (see explanation at the end of Sect. 5). All errors correspond to 90% confidence level.

4. The long term spectral evolution

To avoid systematic errors due to cross-calibration uncertainties between the different instruments we restrict our spectral analysis to the EPIC-pn data. Moreover we use only the eleven EPIC-pn observations of RX J0720.4−3125, which were done in full frame mode with the thin filter. We extracted the pulse-phase averaged spectra from circular source and background regions with

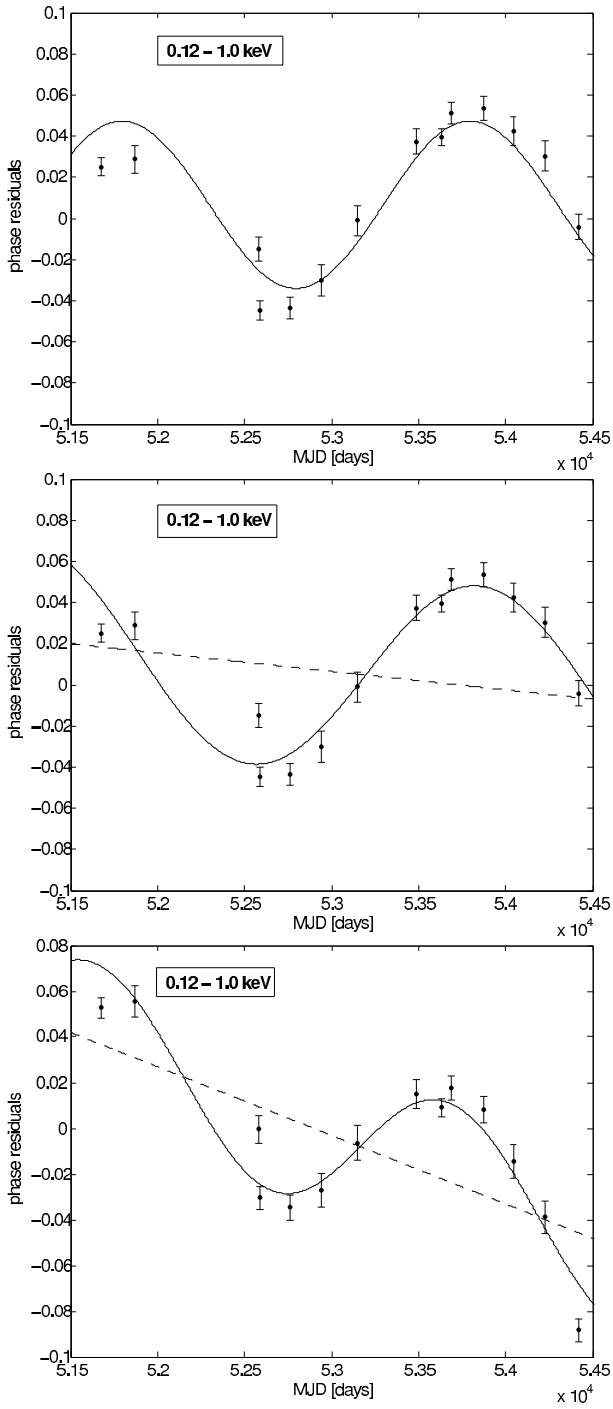

Fig. 8. Phase residuals of RX J0720.4−3125 derived from the EPIC-pn data using the timing solution from Kaplan & van Kerkwijk (2005) fitted with a pure sinusoidal model (top) and a sinusoidal model including a linear term (middle). The fit with the latter model for the timing solution of van Kerkwijk et al. (2007) is shown in the bottom panel. The periods are (5.48 ± 0.33), (7.20 ± 1.50) and (5.59 ± 0.57) yr, respectively, while the values for χ^2/d.o.f. are 59.74/10 (*top*), 43.05/9 (*middle*) and 57.25/9 (*bottom panel*).

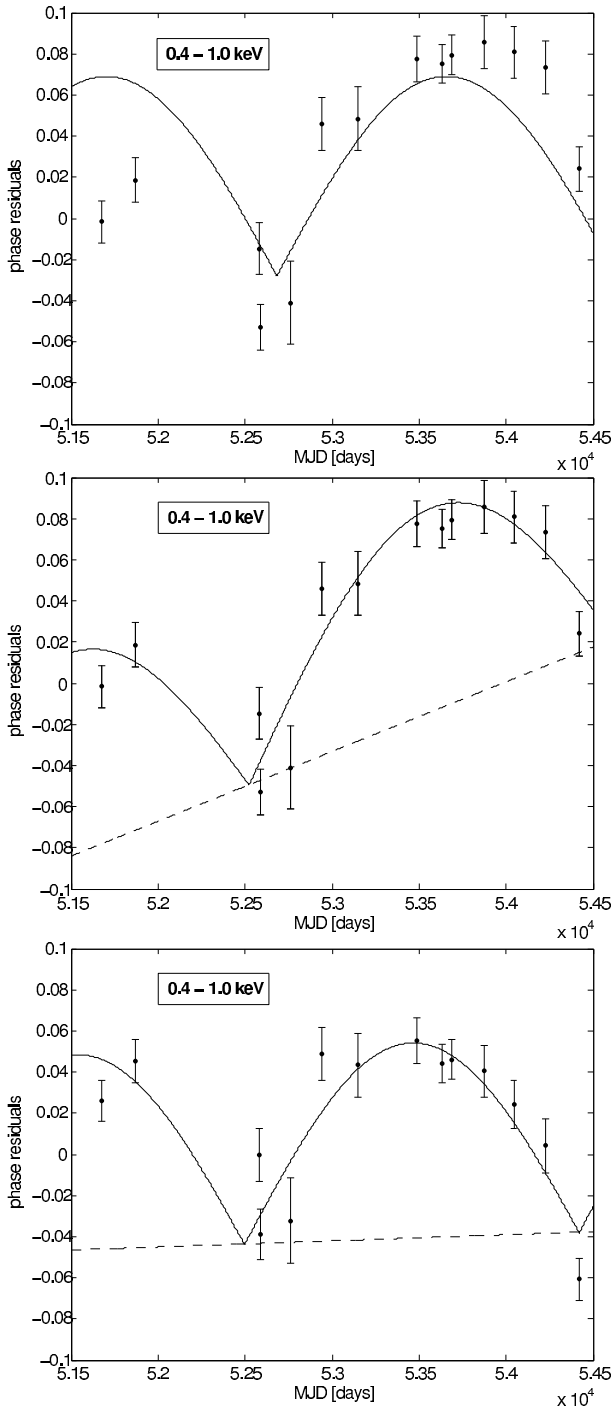

Fig. 9. Phase residuals of RX J0720.4−3125 derived from the EPIC-pn 0.4–1.0 keV data. The error of the phase residual from revolution 622 (around MJD = 52 800 days) was increased by a factor of two (see text). Shown are the best fit models based on different abs(sine) functions and different timing solutions as summarized in Table 2. The derived periods are (10.711 ± 0.058) yr (model B1, *top*), (11.504 ± 0.072) yr (B2, *middle*) and (10.546 ± 0.069) yr (B3, *bottom*).

1′ in diameter, selecting single-pixel events (PATTERN = 0). The spectra were binned to obtain at least 100 photons in each bin. The fits were performed with XSPEC12 and restricted to energies between 0.16 keV and 1.5 keV. We used the blackbody model plus an additive Gaussian line, which represents the absorption feature (negative normalisation). The energy resolution of the instrument is not sufficient to determine the shape of the absorption feature. A Gaussian profile applied multiplicatively yields equally good fits. The feature might also consist of several unresolved lines or have the shape of an absorption edge. Here and below, the errors on the spectral parameters correspond to the 90% confidence level.

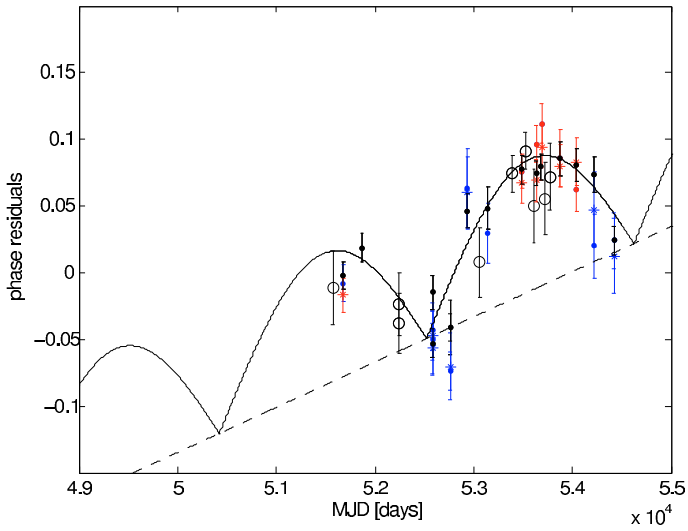

Fig. 10. The phase residuals (only hard band) shown in Fig. 4 together with model B2 derived from the EPIC-pn (hard) data shown in Fig. 9 (middle). Phase residuals from ROSAT and Chandra with errors larger than 0.03 (phase residuals) are excluded.

We linked all model parameters for the spectra of revolution 533 and 534, because the two observations were only two days apart. The line energy, the line width σ and the hydrogen column density $N_{\rm H}$ were linked for all spectra, i.e. we assume that they do not vary with time. All spectra were fitted simultaneously. The best fit parameters are (301 ± 3) eV for the line energy, $\sigma = (77 \pm 2)$ eV and $N_{\rm H} = (1.04 \pm 0.02) \times 10^{20}$ cm^{-2}. For all spectra together we obtain χ^2/d.o.f. = 1.29 with 1767 degrees of freedom. The blackbody temperature kT, the blackbody normalisation (used to calculate the size of the emitting area, assuming a distance of 300 pc) and the line equivalent width EW were free parameters and their best fit values are listed in Table 3. The time evolution of the parameters is drawn in Fig. 11. We also included kT and EW of the three EPIC-pn observations done with different observing mode and different instrument setup in this figure, which were not used for this fit. Because of the cross-calibration uncertainties mentioned above, the blackbody radii obtained from these observations are not reliable and thus not included in Fig. 11, bottom.

As can be seen in Fig. 11, the sine wave form is not a good approximation for the new data. We only can conclude that, if the variation in the spectral parameters is cyclic, the period is larger than the time span of the EPIC-pn observations. Currently it is not possible to predict whether it is periodic or not and if it is periodic, what the shape of the variation might be.

Following H06 we computed pulse phases for each detected event using the timing solution of KvK05. We divided one pulse period into five phase intervals and extracted spectra from each phase interval for each observation. As in the analysis of the phase-averaged spectra, we performed a joint fit to the 55 spectra with the same parameters linked (χ^2/d.o.f. = 1.16 with 6452 degrees of freedom). The change of kT and EW during the pulse period for each of the observations is shown in Fig. 12. As seen before, the parameters evolve counter-clockwise and the long term trend of the parameters, as seen in Fig. 11 continues at all pulse phases. sectionShort term variation

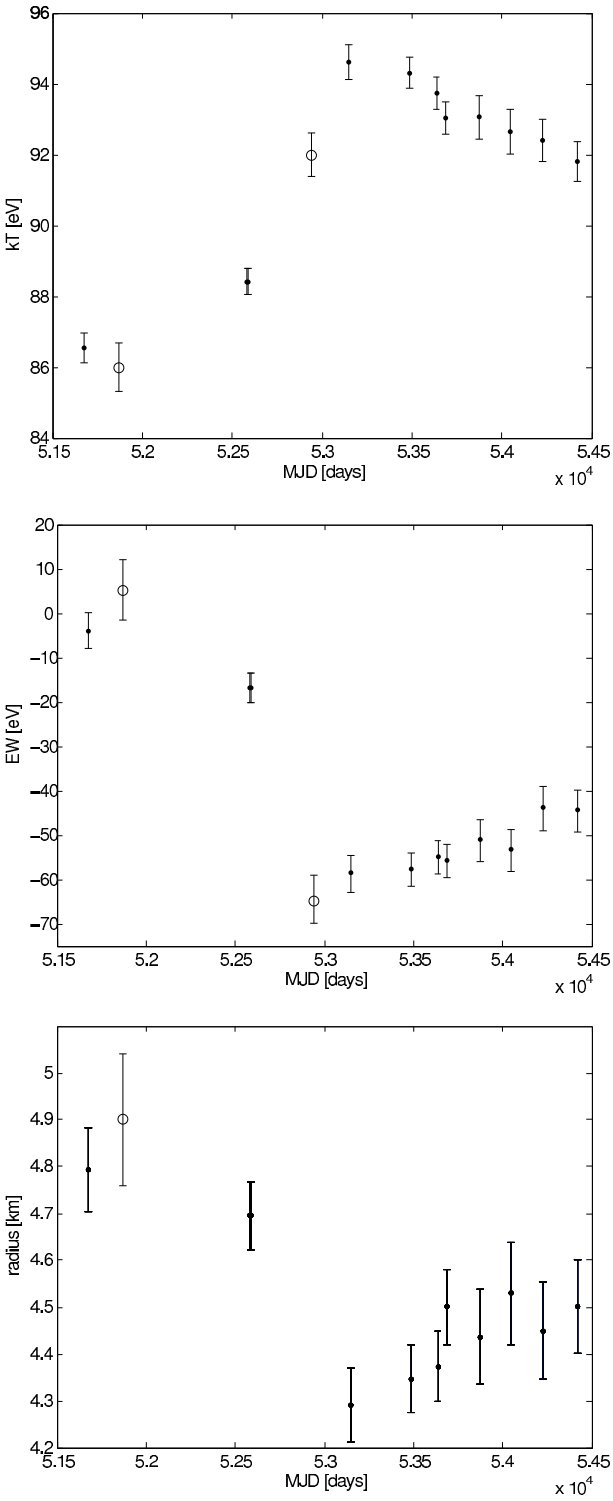

Fig. 11. Long term variations of the pulse phase averaged spectra obtained from the eleven EPIC-pn observations in full frame mode with a thin filter (dots). Open circles show data obtained from the other EPIC-pn observations (see Table 1). Error bars denote 90% confidence level.

5. Discussion

We present new XMM-Newton observations of the isolated neutron star RX J0720.4−3125 performed during our half-year monitoring program in 2006 and 2007. Combining the new data with the previous XMM-Newton data presented by H06 and with Chandra data (KvK05, vK07), we followed the spectral and timing behaviour of the source. As shown by KvK05 and vK07, a phase-coherent timing analysis assuming a constant spin-down of the pulsar yields relatively large phase residuals. Different

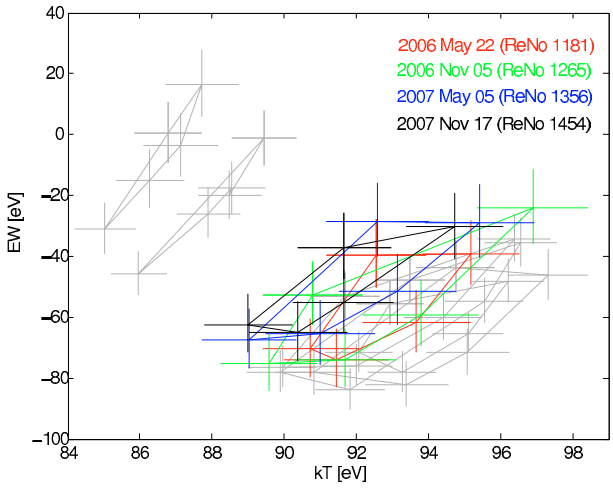

Fig. 12. Phase resolved variations of equivalent width versus temperature. Observations already used for Fig. 6 in H06 are marked in grey. The four new EPIC-pn data are coloured. The error bars denote 90% confidence level.

models have been fitted to these phase residuals invoking a more sudden change in properties (vK07) on one hand or a periodic behaviour (H06 and vK07) on the other hand. Physically, these effects could be interpreted, e.g., by a "glitch" or by precession of the neutron star, respectively.

The analysis of all available data from the different instruments on XMM-Newton and Chandra yields systematic shifts between the phase residuals (Fig. 1). As already noted by Haberl (2007) this is most likely caused by intrinsicaly energy dependent phase residuals and this must be accounted for when using different instruments of different energy response. This is confirmed by our timing analysis using events from the EPIC-pn data in the soft (120–400 eV) and hard (400–1000 eV) energy band separately, which yield systematic phase shifts (Fig. 2). Moreover, the phase shifts between soft and hard photons vary with time. In order to still combine the results from the different instruments, we restricted our analysis to the hard energy band for the three EPIC instruments and for ACIS. The negligible spectral capabilities of the HRC prevented an energy selection and we excluded the ROSAT data completely due to the large errors and alias periods caused by the interrupted observations. This brought the phase residuals from the various instruments in much closer agreement (Fig. 4).

Because of the systematic shifts of the pulse phases on time scales of years, which become visible as phase residuals with respect to the model with constant spin-down of the neutron star, the solutions for $\dot{P}$ strongly depend on the time interval used for the analysis. Only when the observations eventually cover a period significantly longer than the time scale of the phase variations – which is currently not the case – a reliable value for $\dot{P}$ can be derived. This is true if the phase variations are periodic, but also for a sudden event with a long ($\geq$10 yrs) relaxation time. To overcome this problem, we included a linear term into our long term modeling of the phase residuals and investigate two solutions for $\dot{P}$ as inferred by KvK05 (all data solution) and vK07 (all data solutions without glitches). However, we emphasize that both solutions should be regarded as first approximations and that any future timing analysis combining data from different instruments needs to be restricted to narrower energy bands.

Using an abs(sine) function to model the variations of the phase residuals, we obtain periods of 9–15 years with the most reliable values around 9.3–11.5 years for the two fits with the lowest χ^2 (Table 2). The observations still cover less than two "humps" of the abs(sine) function and more data are needed to ultimately verify that the timing behaviour is indeed cyclic and to determine the period more precisely. The energy dependence of the phase shifts (Fig. 2) clearly demonstrates that the long term period covers two humps of the abs(sine). This was not taken into account previously and is at least partly the reason for the shorter periods determined in the past (H06, vK07).

For the spectral analysis of RX J0720.4−3125 it is even more important to avoid systematic differences due to cross-calibration uncertainties between the various instruments. Therefore, we restricted our spectral analysis to the EPIC-pn data taken in full frame CCD readout mode and with a thin optical blocking filter. As in H06 we use a simple absorbed blackbody model including an absorption feature which we assume to be of Gaussian shape. The new XMM-Newton observations show that the inferred spectral parameters continue to change, but do not follow the sinusoidal evolution suggested by the previous subset of data used in H06. Temperature, kT, the apparent radius of the emitting area and the equivalent width, EW, of the absorption line changed more slowly over the years 2006 and 2007 than an extrapolation of the sine model would predict. The spectral data do not allow us to draw any conclusions about periodicity.

The phase lags between soft and hard emission (Fig. 2) suggest the existence of at least two hot regions on the neutron star surface with somewhat different emission characteristics. These hot spots might be associated with the polar caps of the neutron star in a magnetic field. Two hot spots have also been suggested to explain the rotational variations seen in the light curves of RBS 1223 – another M 7 star – in different energy bands (Schwope et al. 2005). To explain the different energy dependence of the two peaks are seen in the pulse profiles of RBS 1223, these authors suggest two hot spots with different size and temperature which are not anti-podal. A similar geometry can in principle also account for the spectral variations seen in RX J0720.4−3125 during its spin period. However, to explain the change in the phase lags over time seen in RX J0720.4−3125, requires a slow apparent movement of the spots relative to each other as seen from the distant observer.

One possible explanation would be free precession of the neutron star as suggested by de Vries et al. (2004) and put forward by H06. In this case the viewing geometry changes and no physical movement of the hot spots on the stellar surface is required. This model is discussed in detail in H06, but as already discussed above, can only be verified when the periodic behaviour is confirmed. The simple, free precession model discussed in H06 was able to account (at least qualitatively) for the long-term evolution of the spectral parameters over the period examined (May 2000–November 2005) and also by invoking two non-antipodal caps for the peculiar intensity-hardness anti correlation with spin phase. Although this was not discussed in H06, the model predicts a cyclic variation in the phase residuals due to the change in the pulse shape (of the phase of the light curve maximun in particular) over the precession period. Since the spin-phase dependence of the hardness ratio changes along the precession cycle (this can be also seen in the lower right panel of Fig. 5 in H06), one expects that the phase residuals and their variation over time are not the same in different energy bands. Indeed, as we checked, the free precession model outlined in H06 is able to reproduce (again, qualitatively) the properties of the observed residuals (see Fig. 2). The highly non-sinusoidal pattern of the spectral parameters,

which clearly emerges from the latest data (see Fig. 11), however, may be, an issue. In order to explain the fast change around MJD = 52 800 days one needs to invoke the coming into view of a rather small "spot" with angular size $\sim \Delta t / P_{\rm prec} \approx 10^\circ$ where we take $\Delta t \sim 500$ d as the timescale over which the rapid change occurred and $P_{\rm prec} \sim 10$ yr. However, the presence of such a small emitting region produces a pulse shape which is not in agreement with the observed one. It is still under debate whether free precession can continiue for more than a few hundred cycles (Link 2006). If this is the case and RX J0720.4−3125 is precessing, then the precession needs to be powered by some mechanism. Precession caused by an unseen sub-stellar companion can probably be excluded on the basis of the current upper limit on its mass obtained by Posselt et al. (2008) from a search for orbiting objects around RX J0720.4−3125 (see also the discussion on PSR B1828-11 by Liu et al. 2006).

Alternatively, the regions on the surface responsible for the hard and soft emission may physically change their locations or their emission properties. A slow rearrangement of the magnetic field may change the local angle between the surface normal and the field, influencing the emission pattern, and the heat transport in the crust. In such a picture the rearrangements do not need to be periodic, but a different physical mechanism is required to explain it. A glitch (vK07) may be one possibility. The occurrence of such a sudden event might be supported by the relatively fast change observed in the spectral parameters around MJD = 52 800 days (see Fig. 11) and the more gradual evolution afterwards which resembles a relaxation process. However, the EPIC-pn small window mode data from 2003 (satellite revolution 711) and in particular the RGS data indicate a more gradual temperature increase before MJD = 52 800 days (de Vries et al. 2004). The small window mode data (thick and medium filter) was not used here at all and only partly by H06, because of a normalisation discrepancy between small window and full frame mode in the EPIC-pn calibration. This affects the inferred black body radius, but not the temperature. It should also be noted that the basic characteristic behaviour in the spectral variations was not altered around this date. The changes in kT, radius and EW seen on long term time scales are also seen during the neutron star rotation, before and after the putative event (Fig. 12 and compare to Fig. 4 in H06) and the total X-ray flux stays nearly constant within a few per cent (H06). The amplitude of the EW variation during the spin period did not change over the years, only the mean level evolves. In the case of the temperature, both amplitude and mean level evolve on long time scale, but this evolution is visible in the EPIC-pn spectra during all observations, first slowly and then fast with a large change around MJD = 52 800 days. Therefore, we regard a sudden event like a glitch as an unlikely cause for the (more gradual) spectral variations.

In conclusion, the timing and spectral properties of RX J0720.4−3125 are both consistent with the existence of at least two hot spots with different temperature on the surface of the neutron star. Whether the long term changes are periodic requires further monitoring. A simultaneous modeling of spectral and timing parameters is in progress and should eventually yield a more detailed temperature map of this unique isolated neutron star.

Acknowledgements. The XMM-Newton project is supported by the Bundesministerium für Wirtschaft und Technologie/Deutsches Zentrum für Luft- und Raumfahrt (BMWI/DLR, FKZ 50 OX 0001) and the Max-Planck Society. M.M.H. and V.H. acknowledge support by the Deutsche Forschungsgemeinschaft (DFG) through SFB/TR 7 "Gravitationswellenastronomie". The work of R.T. is partially funded by INAF-ASI through grant AAE TH-058 and S.Z. acknowledges the STFC for support through an Advanced Fellowship.

References

Blaschke, D., & Grigorian, H. 2007, PrPNP, 59, 139
Cropper, M., Zane, S., Ramsay, G., et al. 2001, A&A, 365, 302
Cropper, M., Haberl, F., Zane, S., & Zavlin, V. E. 2004, MNRAS, 351, 1099
de Vries, C. P., Vink, J., Méndez, M., & Verbunt, F. 2004, A&A, 415, L31
Haberl, F. 2005, MPE Rep., 288, 39
Haberl, F. 2007, Ap&SS, 308, 181
Haberl, F., Motch, C., Buckley, D. A. H., et al. 1997, A&A, 326, 662
Haberl, F., Turolla, R., De Vries, C. P., et al. 2006, A&A, 451, L17 (H06)
Jansen, F., Lumb, D., Altieri, B., et al. 2001, A&A, 365, L1
Kaplan, D. L., Kulkarni, S. R., van Kerkwijk, M. H., & Marshall, H. L. 2002, ApJ, 570, L79
Kaplan, D. L., & van Kerkwijk, M. H. 2005, ApJ, 628, L45 (KvK05)
Kaplan, D. L., van Kerkwijk, M. H., & Anderson, J. 2007, ApJ, 660, 1428
van Kerkwijk, M. H., Kaplan, D. L., Pavlov, G. G., & Mori, K. 2007, ApJ, 659, L149 (vK07)
Link, B. 2006, A&A, 458, 881
Liu, K., Yue, Y. L., & Xu, R. X. 2007, MNRAS, 381, L1
Page, D., & Reddy, S. 2006, ARNPS, 56, 327
Page, D., Geppert, U., & Weber, F. 2006, NuPhA, 777, 497
Posselt, B., Neuhäuser, R., & Haberl, F. 2008, A&A, submitted
Schwope, A. D., Hambaryan, V., Haberl, F., & Motch, C. 2005, A&A, 441, 597
Strüder, L., Briel., U., Dennerl, K., et al. 2001, A&A, 365, L18
Trümper, J. E., Burwitz, V., Haberl, F., & Zavlin, V. E. 2004, NuPhS, 132, 560
Turner, M. J. L., Abbey, A., Arnaud, M., et al. 2001, A&A, 365, 27
van Kerkwijk, M. H., & Kaplan, D. L., 2007, Ap&SS, 308, 191
Vink, J., de Vries, C. P., Méndez, M., & Verbunt, F. 2004, ApJ, 609, 75
Zane, S., Haberl, F., Cropper, M., et al. 2002, MNRAS, 334, 345